The operation of a low-power cylindrical Hall thruster with zinc as the propellant

IEPC-2019-A920

Presented at the 36th International Electric Propulsion Conference
University of Vienna • Vienna, Austria
September 15-20, 2019

S. Dworski[1], J. Martin[2], C. Ryan[3], E. Dyer[4],
Faculty of Engineering and the Environment, University of Southampton, United Kingdom

and

A. Demaire[5], V. Garcia[6]
*OHB Sweden AB, S*olna, SE-171 04, *Sweden*

There is a strong interest to develop electric propulsion systems that utilize alternative propellants to xenon, both for smaller platforms with tighter budget, mass, and volume constraints, or for larger satellites that may otherwise deplete the world market resource. This is leading to the development of high performance electric propulsion systems, for example Hall Effect Thrusters, which can operate on alternative propellants. Hall Thrusters (HTs) have been shown to function with a wide range of propellants including xenon, krypton, iodine, and more exotic propellants such as zinc, magnesium and bismuth. Their relatively simple annular topology makes them well suited to miniaturisation, however reduced component size has implications for the strength of the magnetic field, erosion of the channel, and the level of heating present. The Cylindrical Hall Thruster (CHT) was proposed to address these issues, using a recessed annular channel to reduce the surface-to-volume ratio and a cusp magnetic field to contain the electrons. A collaborative project between the University of Southampton and OHB Sweden has begun to characterise a low-power CHT using firstly Krypton, and then to compare the performance to when using zinc as the propellant.
The paper presents the results of the characterisation of the CHT-100 thruster using krypton, and development of the thruster for operating with zinc. The design of the CHT-100 is described, and also the setup of the test campaign used to evaluate the thruster performance, with a pendulum thrust balance used to accurately record the thrust produced and therefore efficiency. Results from operating the CHT-100 on krypton are discussed.
The in depth characterization of a propellant delivery system using zinc as the propellant are described. This involves thermal analysis of the system,
Further, the design of a low power (100 – 200 W) Hall Effect Thruster is discussed. The design process is described, including validation that it is capable of operating on alternative propellants. The manufactured thruster is illustrated and the magnetic field demonstrated to be that which is required.

Nomenclature

A	=	Area; empirical coefficient
B	=	Empirical coefficienct
C	=	Empirical coefficient
C_{T1}, C_{T2}, C_P and C_B	=	Constants of proportionality
d	=	Channel mean diameter

[1] Undergraduate student, University of Southampton, sd1g16@soton.ac.uk
[2] Postgraduate student, University of Southampton, jm2u18@soton.ac.uk
[3] Lecturer, Astronautics Group, University of Southampton, c.n.ryan@soton.ac.uk
[4] Undergraduate student, University of Southampton, ecd1g15@soton.ac.uk
[5] Head of Propulsion Team, OHB Sweden AB, alain.demaire@ohb-sweden.se
[6] Propulsion Engineer, OHB Sweden AB, vincent.garcia@ohb-sweden.se

D	=	Empirical coefficient
g_r	=	Radial ion flux to the walls
h	=	Channel width
I_{EM}	=	Electromagnet current
k_B	=	Boltzmann constant
L	=	Channel length
$\dot{m}$	=	Mass flow rate
M	=	Molecular mass
n_c	=	Channel material density
n_e	=	Number density of electrons
n_i	=	Ion density
P_c	=	Chamber pressure
P_v	=	Vapour pressure
q	=	Elementary charge
t_{life}	=	Thruster lifetime
T	=	Temperature
U_d	=	Discharge voltage
v_B	=	Bohm velocity
v_e	=	Electron thermal velocity
v_n	=	Thermal velocity of neutral atoms, , and v_e is the electron thermal velocity
v_i	=	Ion velocity
ε	=	Ion energy
θ	=	Beam divergence
δh_c	=	Channel wall thickness
η_θ	=	Beam angle efficiency
η_{++}	=	Doubly charged ion effciency
λ_i	=	Mean ionisation length
σ_n	=	Electron impact ionisation cross section of the neutral atom
$Y(\varepsilon, \theta)$	=	Sputtering function

I. Introduction

The Hall Effect Thruster (HT) possesses a significant flight heritage, and has become the choice for orbit raising of satellites within Earth Orbit, encompassing several hundred kilogram microsatellites to several tonne geostationary all electric platforms. It offers high specific impulse, but at a greater thrust to power ratio and thrust density than a gridded ion thruster.

The Hall Thruster is in particular viewed as highly suitable for the orbit raising of Low Earth Orbit microsatellites, as part of a constellation. Various microsatellite constellations are currently under consideration, including SpaceX (3000 satellites), Amazon (3200 satellites), and OneWeb (600 satellites). The majority of these satellites will require a significant change to the semi major axis after launch vehicle deployment, with most requiring a significant attitude increase. This altitude change is likely unfeasible using traditional chemical monopropellant thursters, therefore driving a need for small electric propulsion suitable for this microsatellite class.

Consequently the number of satellites that will be using Hall Thrusters in Low Earth Orbit is expected to increase dramatically in the next five to ten years. Hall Effect Thrusters operate through the electrostatic acceleration of ions of typically xenon. Xenon is typically used as the propellant of choice within Hall Effect Thrusters. It is inert, heavy element, that also possesses a high ionization cross section and the lowest first ionization potential of the stable noble gases. Of the noble gases, xenon also possesses the highest storage density when stored under pressure, typically stored within tanks at 1.5 g/cm3 under a pressure of 14 MPa. This high density is desirable for volume constrained systems such as microsatellites. These factors combine to make xenon a highly suitable propellant; it is inert, only moderate thermal control is required, it is relatively straight forward to ionize, and offers a high thrust for a given power.

The world production of xenon per year is estimated to be 53,000 kg [1], with the current use within spacecraft electric propulsion accounting for approximately 10 % of the current demand. There is estimated to be 2 x 10^{12} kg of xenon in Earth's atmosphere, providing enough available propellant to satisfy the satellite, but the demands from the growth of a new xenon market may put significant pressure on the xenon production.

If one microsatellite requires 10 kg of xenon propellant for orbit raising (given a satellite initial mass of 230 kg, and a specific impulse of 1500 seconds, this results in providing a change in velocity of 650 m/s), then the planned constellations of 600, 3000, and 3236 satellites from OneWeb, SpaceX and Amazon will require 130 % of the yearly production, or 13 % over ten years. If this demand is combined with the demand for for xenon for the electric propulsion requirements of other spacecraft, for example geostationary, or other missions such as the lunar gateway, then there could be a significant effect on the price and availability of xenon.

Therefore, it is worth considering alternative propellants for the small Hall Effect Thrusters that will be utilized on board these constellations. This is driving technological and commercial innovations, with various companies (Orbion Space Technology, Apollo Fusion, Busek, Sitael) actively investigating alternative propellants within Hall thrusters. This alternative propellant consideration is clearly demonstrated by the launch of the first 60 satellites that will form the SpaceX Starlink constellation, each including a small (likely ≤1000 W) Hall Effect Thruster with krypton as the propellant.

Consequently, there exists a strong desire to develop propellants alternative to xenon that are suitable for Hall Effect Thrusters. Various alternative propellants exist, including other noble gases[2], iodine[3,4], mercury or metallic propellants such as bismuth[5,6], zinc[7,8], cadmium, and magnesium[9]. Many of these have particular advantages over xenon, for example lower ionization, or in particular a higher storage density. If an alternative propellant can be found that offers particular advantages over xenon, without too greater detrimental effects such as toxicity or lower performance, then it would seem likely that it can well compete with xenon as the propellant of choice within small Hall thrusters.

This paper will describe the ongoing experimental investigations of alternative condensable propellants in Hall Thrusters at the University of Southampton. In particualr metalic propellants such as zinc and magnesium are the current focus. The work to develop a cylindrical hall thruster is described, design and tested on a pendulum thrust stand. The ongoing development of a propellant delivery system capable of delivering controllable amounts of zinc and magnesium propellant to a Hall thruster is described, including details of the delivery system design, and experimental sublimation of the zinc propellant. Finally the detailed design and manufacture of an annular Hall Thruster designed to operate at around 100 W with conensable metallic propellants is described.

II. Operation of Cylindrical Hall Thruster on krypton

A. CHT-100 Thruster

A small cylindrical Hall thruster (CHT) was developed at the University of Southampton[10], to act as a simple low cost test bed for work on alternative propellants. It is of a relatively typical CHT design, as that investigated by various other studies[11-13]. The CHT was designed to operate at an input power of 100 – 300 W, and consists of an annular section, of 12 mm inner diameter, 24 mm outer diameter, with the depth of the annular and cylindrical sections being 18.5 and 20.5 mm respectively. The CHT-100 is designed to operate in two configurations; electromagnet (EM) mode, and permanent magnet (PM) mode, as illustrated in Figure 1. In EM mode, the thruster uses two electromagnets; a large solenoid to produce the primary magnetic field, and a smaller solenoid working in opposition to the primary field to provide a cusp field. In PM mode, the larger solenoid is replaced with two samarium-cobalt ring magnets (SmCo-26), and the steel outer wall is replaced with aluminium. In both configurations, a thin steel plate separates the smaller solenoid from the larger solenoid/permanent magnet. This creates a magnetic mirroring point between the smaller solenoid and the larger solenoid/permanent magnet, trapping electrons between this point and the magnetic mirror point at the central pole. The magnetic mirror effect, combined with a possible ExB effect occurring when the field is perpendicular to the electric field, results in electron confinement and the resulting ionization and acceleration of ions.

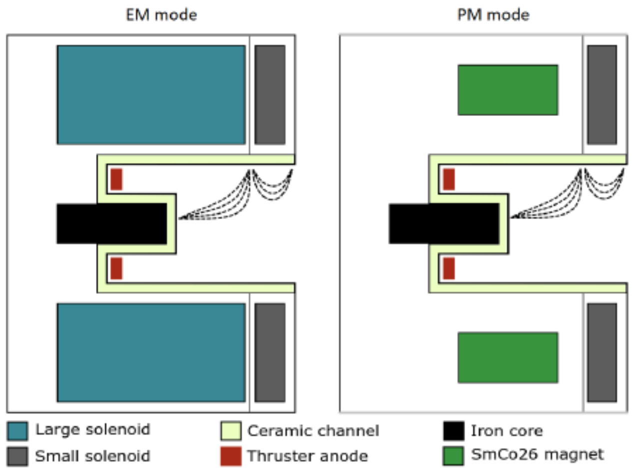

Figure 1. The CHT-100 thruster in electromagnet and permanent magnet configurations.

Simulations of the magnetic structure of the thruster were completed using FEMM software. In both modes peak magnetic field occurs in the central region of the thruster, near the iron core. In EM mode, the peak magnetic field is 0.15 T, similar to other CHT devices [13,14] While operating in PM mode the magnetic field is 0.25 T and similar values have been reported for CHT devices operating with permanent magnets[15].

The thruster was characterised within the David Fearn vacuum facilities at the University of Southampton. The chamber is 2 m in diameter and 4 m in length with two turbo-pumps (2100 L/s of N2 each) and two cryopanels (15,000 L/s of Xe each), which can achieve a base pressure of 9.8×10^{-7} mbar, and an operating pressure of the low 10^{-5} mbar range with a flow of 10 sccm of krypton.

The performance was characterised using a pendulum thrust stand similar to others developed previously[16], and illustrated in Figure 2.

An Intlvac HCES-5000 Hollow Cathode is used as the electron source. It should be noted that the performance of this cathode is relatively poor, requiring a flow rate of 8 sccm for operation. Consequently only the anode power and efficiency are considered.

The thrust and anode efficiency from using the EM version of the CHT-100, as measured during varying the anode power from approximately 100 to 300 W, is illustrated in Figure 3. The data is summarized in Table 1. Generally the data demonstrated a reasonable performance, but somewhat low when compared to other cylindrical hall thruster of similar designs. The performance was deemed adequate for operating with condensable propellants, but it was also decided to design and manufacture a full annular Hall Effect thruster, as discussed in Section V.

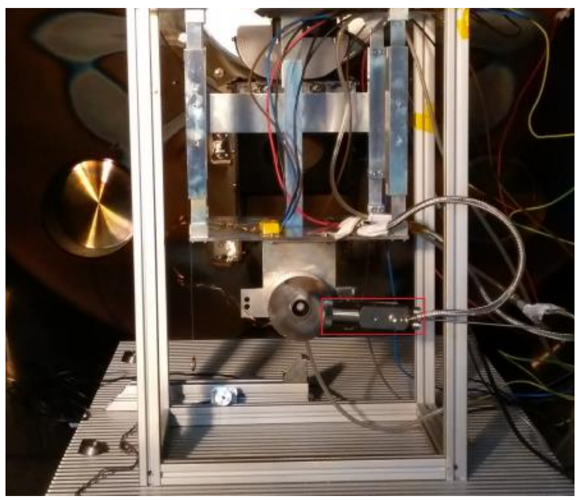

Figure 2. CHT-100 thruster setup on thrust stand within vacuum chamber facility.

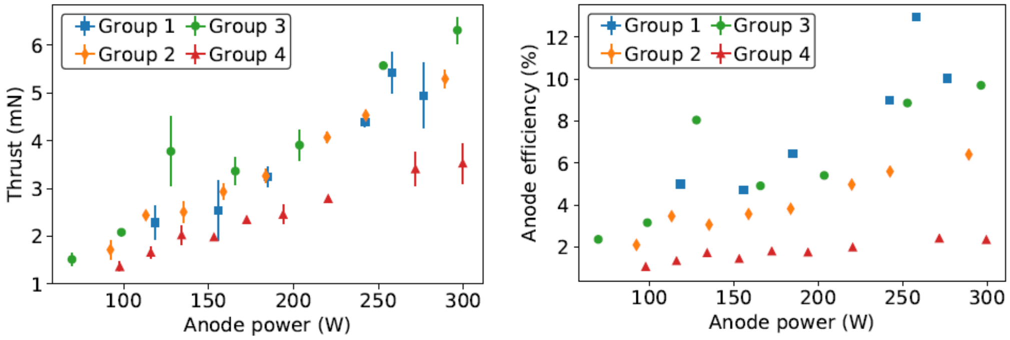

Figure 3. Thrust and anode efficiency produced by the CHT-100 recorded by students during the teaching lab. Group 1: $\dot{m}$ = 7 sccm, I_{EM} = 1.75A. Group 2: $\dot{m}$ = 12 sccm, I_{EM} = 1.3A. Group 3: $\dot{m}$ = 11 sccm, I_{EM} = 1.6A. Group 4: $\dot{m}$ = 14 sccm, I_{EM} = 1A.

Table 1. CHT-100 measured performance with data as illustrated in Figure 3.

#	**Flow rate (sccm)**	**Thrust (mN)**	***Isp (s)***	**Efficiency (%)**
1	7	2.29 – 5.43	529 – 1254	4.7 – 13
2	12	1.71 – 5.3	230 – 714	1.7 – 5.3
3	11	1.51 – 6.32	222 – 928	1.5 – 6.3
4	14	1.36 – 3.53	157 – 407	11.4 – 3.5

III. Design of propellant delivery system suitable for zinc and magnesium

A. Determination of Temperature Requirements

For the use of condensable propellants with HETs, the propellant delivery system must be able to generate a specific mass flow rate that has been identified as nominal for thruster operation. Furthermore, there should be minimal deviation fluctuation in the flow rate in order to maintain thruster conditions so that the performance can be well predicted. To determine the required propellant temperature that will achieve the necessary ow rate requires analysing the temperature dependence of the sublimation process. The mass flow rate of sublimation in units of kg/s for a perfect vacuum is given as[6]:

$$\dot{m} = \frac{P_v}{\sqrt{\dfrac{2\pi\, k_B T}{M}}} A \tag{1}$$

where P_v is the element's vapour pressure, M the molecular mass, k_B the Boltzmann Constant, T temperature, and A the exposed area of the condensed phase. Conversion from kg/s to sccm is given by:

$$1\,\text{sccm} = 4.477962 \times 10^{17} \cdot M \cdot \dot{m} \tag{2}$$

The vacuum chamber pressure P_c will impact the ow rate and must be considered. The net flow rate in sccm for a non-perfect vacuum can be calculated as:

$$\dot{m} = \frac{P_v - P_c}{4.4477962 \times 10^{17} \sqrt{2\pi\, M k_B T}} A \tag{3}$$

This shows that when the propellant vapour pressure exceeds the ambient pressure there will be a net flow of gaseous propellant. The vapour pressure can be increased by heating of the propellant. C. Alcock presents the general form for the temperature dependence of the vapour pressure of metallic elements[17]:

$$\log P_v = 5.006 + A + BT^{-1} + C \log T + DT^{-3} \tag{4}$$

where *A*, *B*, *C* and *D* are empirical coeficients specific to each metallic element that are provided in the same paper.

The propellant tank being used for the condensable propellant testing is shown in Figure 8 below. The tank has a flange which enables cylindrical slugs of zinc propellant to be inserted inside the tank. The top of the propellant slug is exposed and is the surface where sublimation will occur. The radius of the propellant slug used for testing was 15.7 mm which determined the value of *A*.

Figure 4 shows the results of employing the equations above to the tank dimensions of the propellant delivery system (PDS). The vacuum chamber pressure was set at 10^{-4} mbar, which is approximately the pressure that can be achieved using the chamber this work will be carried out in. The results show no flow occurs until a threshold temperature is reached, after which further heating increases the flow.
As expected, magnesium has higher temperature requirements to achieve the same flow rate as zinc due to its lower vapour pressure. The estimated temperatures to achieve magnitudes of flow typically required for HET operation are given in Table 2.

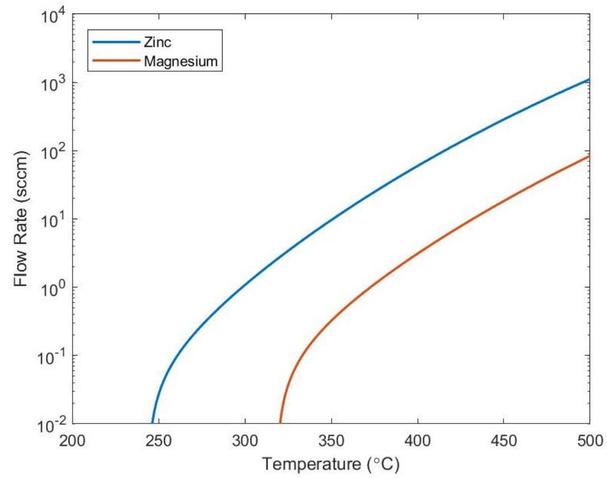

Figure 4. Temperature dependence of the flow rate of sublimated condensable propellants for a chamber pressure of 10^{-4} mbar.

The required temperatures for both zinc and magnesium are feasible to achieve without extremely high heating powers. The melting points of zinc and magnesium are approximately 420 °C and 650 °C respectively. Liquefying the propellant must be avoided for the condensable PDS as this will make it much harder to remove propellant from the tank once it has cooled and solidified. The margin between the required propellant temperatures and melting point is much smaller for zinc than magnesium so greater care must be taken to avoid melting during zinc testing.
From these results the maximum temperature variation to restrict the flow rate fluctuation within a boundary could be determined. To achieve 10 ±0.5 sccm, the temperature variation must remain less than 1.3 °C and 1.5 °C for zinc and magnesium respectively. This requires a precise thermal control system that can minimise the amplitude of temperature oscillation of the propellant.

Table 2. Estimate of propellant temperature requirements for generation of flow rate values for zinc and magnesium.

Flow rate (sccm)	Required Temperature (°C)	
	zinc	magnesium
5	334	413
10	351	432
15	361	444

After metallic vapours have been produced by sublimation, it is vital to ensure that no condensation occurs at any point within the feed line between the tank and thruster. Condensation will lead to blockages and an insufficient flow rate delivered to the thruster. There is limited literature regarding the surface temperatures required to prevent condensation of the metallic vapours, however, an investigation into alternative propellants by A. Kieckhafer states that the condensable propellant feed system must be maintained at a temperature above the melting point of the propellant to prevent condensation[18]. This is supported by the methodology used for the feed system being developed for the iSat HET that uses iodine. For this system they state the propellant tank is heated to 90 °C whilst the feed lines are held at a minimum of 120 °C. The feed line temperature is just above the melting point of iodine at 114 °C which supports the statement made by Kieckhafer. At 420 °C, the melting point of zinc is only 70 °C higher than the temperature required of the tank which is feasible to achieve using low power heating. However, the operation of magnesium propellant would require the feed temperature to be held over 650 °C which is significantly higher than the required propellant temperature and introduces technical challenges to generate and sustain these temperatures within the power constraints of a microsatellite.

B. Thermal Mount Design

For the condensable propellant delivery system, a feed system that was thermally isolated needed to be developed. Further it was conceived to attempt to measure the flow rate using high accuracy load cells (Tedea-Huntleigh Model 1004), thus allowing for specific impulse calculations when using a thrust balance. These load cells are rated to 45 °C and their measurements are temperature dependent with a ±0.004% /°C and ±0.001% /°C temperature effect on the sensor zero point and output respectively. Therefore the load cells needed to be well isolated from the propellant tank. This was resolved by designing an S-shaped mount from Macor ceramic, with the small propellant tank mounted to the top (Figure 5 and Figure 6). Some radiation shielding was also utilized to further protect the load cells.

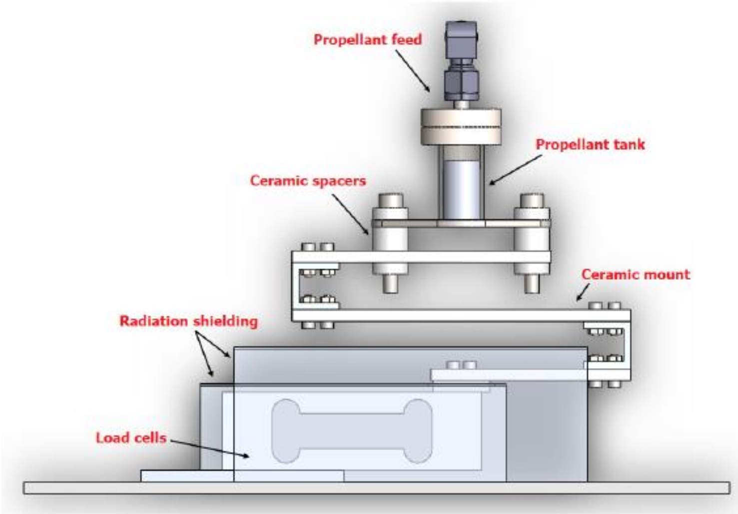

Figure 5. Thermal Mount Design.

COMSOL was used to simulate the experimental conditions required for the sublimation of both zinc and magnesium to verify that the load cell temperatures should remain within operating limits. Figure 7 shows the results for zinc operation at 15 sccm. It was assumed that the propellant temperature will be approximately equal to the tank temperature at thermal equilibrium. Therefore, the propellant tank surface was set at 361 °C and the feed line surfaces set at the zinc melting point. The same scenario was then simulated for magnesium operation, using the required tank temperature for 15 sccm and magnesium melting point as temperature references. From these results, the hottest temperatures reached by the load cells at thermal equilibrium are 25.4 and 19.1 °C for zinc and magnesium respectively, within the load cell limits.

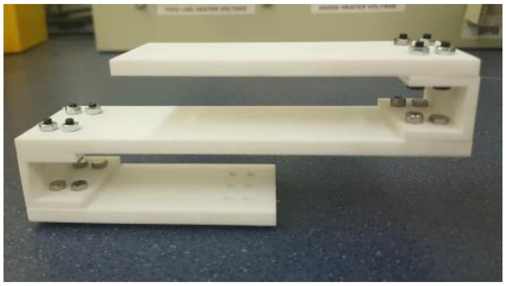

Figure 6. Machined Macor ceramic mount.

During experiments, the PDS and baseplate will be attached to the vacuum chamber which will effectively act as a thermal reservoir that grounds the temperature of the base of the system to room temperature. In each COMSOL simulation, the parts are modelled as floating in vacuum which does not consider this heat transfer path, however, the large base plate is effective at dissipating most of the remaining heat to emulate this effect.

Another source of error in these models is the surface emissivity of the components. Radiative heat dissipation is crucial to ensuring that the heat is drastically mitigated between the heated components and the load cells. Surface emissivity is highly dependent on the surface quality of a material. As such, the values used for the simulations will not be entirely representative of the physical behaviour.

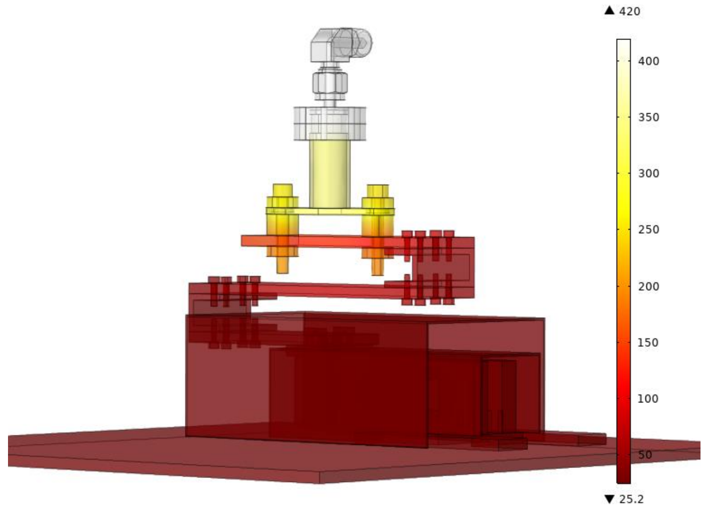

Figure 7. Temperature profile of the PDS for zinc operation of 15 sccm.

Figure 8. The manufactured propellant tank, top flange of propellant tank, and simple feedline.

C. Thermal Control System

Thermal control of the three heaters used for the propellant tank, propellant feed line, and a heater inserted into the central pole of the CHT-100 was required. This was completed through the use of a feedback loop provided by three thermocouples in situ. The heaters used consisted of heater tape types, operated using a 110 V AC power signal.

The feedback loop was initially attempted using a proportional, derivative and integral (PID) system, but this proved difficult as PID control is complicated by an AC power supply. Instead a simple ON/OFF system was created, as illustrated in Figure 9. One of the three control circuits used is schematically illustrated in Figure 10.

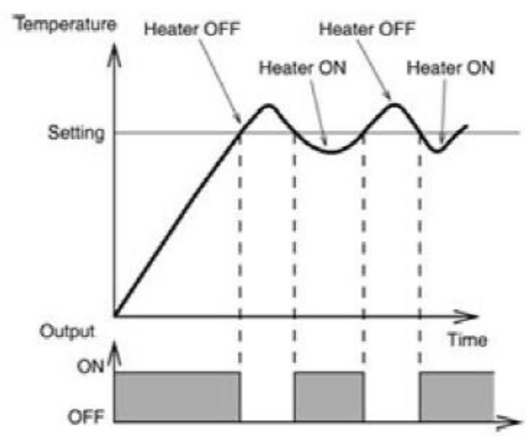

Figure 9. ON/OFF control behaviour utilized on control system for heaters.

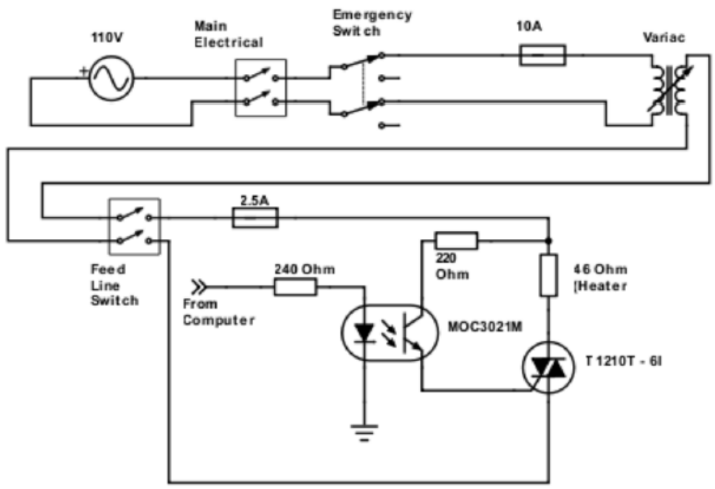

Figure 10. Control circuit for the AC feed line heater.

IV. Operation of condensable propellant delivery system

The operation of the condensable propellant setup was completed within a small vacuum chamber, with a diameter of 450 mm, and length of 500 mm. The chamber was fitted with a roughing and diffusion pump, and obtained a base pressure within the 10^{-5} mbar range whilst during operation.

The objective of the first condensable propellant delivery testing was to produce a controllable and amount of zinc. To facilitate this, the CHT-100 thruster was not attached to the propellant tank and feedline, and instead a simple zinc trap was utilized to capture the zinc output from the PDS. The tank and feedline were wrapped within two heater tapes, with an insulating wrap then used around the heater to attempt to reduce the amount of radiative loss.

Figure 11 illustrates an initial operational run of heating up the feedline temperature to a set temperature of 300 ^{o}C, using the simple ON OFF feedback control. Although an oscillatory temperature effect was noticed of ±5 ^{o}C, the results were deemed promising, and further refinement could lead to greater control.

Initially, with a zinc rod inserted into the propellant tank, the temperature of the propellant tank was increased to the 330 to 370 ^{0}C, identified as the likely temperatures required for the propellant evaporation to occur from the solid piece of zinc, as detailed in Table 2. The feedline was kept at 50 degrees Celsius above the propellant tank temperature.

However no noticeable zinc was evaporated from the propellant tank at these temperatures. To gain some understanding as to why this was the case, a hole was drilled into the bottom of the propellant tank, and a thermocouple was inserted into the tank, and then into a blind hole drilled into the bottom of the zinc rod. The thermocouple was sealed into the tank through the use of Swagelok fittings.

The thermocouple directly making contact with the zinc rod, identified that the zinc rod was approximately 150 top 200 degrees Celsius below the temperature that the thermocouple on the outside of the tank was identifying. Therefore the propellant tank temperature was incrementally increased until zinc was produced.

The initial design also utilized a 1/8” outer diameter pipe as the feedline, with an inner diameter of 1.6 mm. Using this small i.d. pipe though proved to be a disadvantage to zinc gas leaving the PDS. To resolve this issue a larger ¼” was instead used, with an inner diameter of approximately 3 mm.

Through the use of a larger feedline pipe, and higher temperatures measurable amounts of zinc were

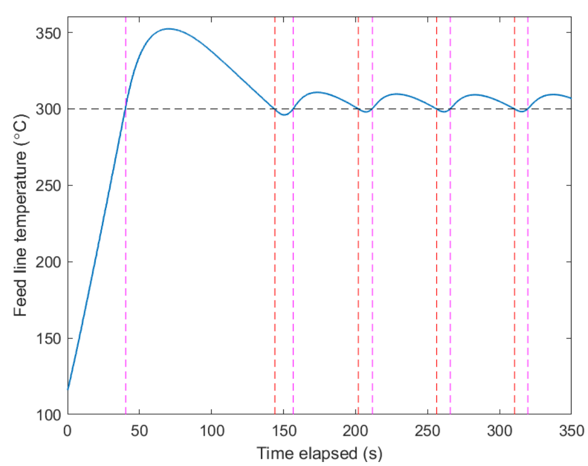

Figure 11. Feed line temperature behaviour under ON OFF control for required temperature of 300 ^{o}C. Heater on at t = 0. Magenta line: heater on; red line: heater off.

produced. The mass decrease of the propellant tank at different temperatures is illustrated in Figure 12. The test was operated for 80 minutes. The data is also summarized in Table 3.

A propellant tank temperature of 570 °C was required to produce a measurable level of zinc. As the temperature was further increased, a slightly increasing amount of zinc propellant was produced, until a temperature of 610 °C was reached where in the mass outputted, and correspondingly the flow rate, increased dramatically. The reason for this increase remain unclear; it was suggested that it may be a result of the surface area of the propellant increasing during the propellant testing, and therefore the mass flow rate increasing. However this possibility was dismissed after the flow rate decreased again once further tests at lower temperatures were completed. Instead it is hypothesised that there is a phase change of some type occurring, perhaps the zinc approaching melting, and this increasing the evaporation rate, or perhaps the flow of gas changing from a molecular flow to a viscous flow. Future work will be conducted to help to understand this phenomenon further.

In summary an adequate amount of zinc gas was produced to allow for testing with a small Hall thruster. Time constraints did not allow for the complete testing with a Hall thruster operating on zinc, but it is hoped that this can be completed within the next several months, allowing with refinement of the propellant delivery system, and temperature control.

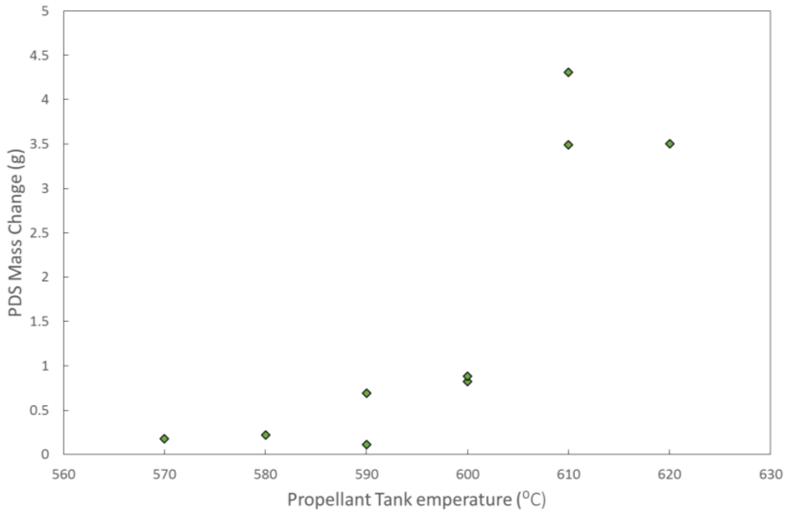

Figure 12. Mass decrease of whole PDS system at different tank temperatures. The feedline temperature was held at 50 °C above the propellant tank temperature. Each test of 80 minutes of duration.

Table 3. Mass lost from zinc propellant delivery system, and measured mass flow rate over 80 minute test.

Propellant Tank Temperature (° C)	Total mass lost from PDS, mg	Flow rate, sccm
570	180	0.80
580	220	0.98
590	690	3.07
600	820	3.65
610	4310	19.19
590	1140	0.51
600	880	3.92
610	3490	15.54
620	3500	15.58

Images of the zinc propellant tank before, during, and after the testing are illustrated in Figure 13. The piece of zinc changed from a smooth surface to a rough crystalline structure, and also small nodules of the propellant formed on the side walls.

Figure 13. Illustration of the propellant tank before the tests, after the initial tests, and at the end of the testing.

V. Design and manufacture of 100 W Hall Effect Thruster

It was decided to develop a small annular Hall thruster, to complement the CHT-100 and hopefully offer an increased performance, in particular efficiency. The thruster was developed using the the scaling laws outlined by K. Dannenmeyer and S. Mazouffre[19,20]. These scaling laws were developed using a database of over 33 existing HETs to determine the proportionality coefficients for each of various thruster dimensions. They enable the optimal thruster geometry to be calculated for a given input power *P* and output thrust *T*. These scaling laws follow as:

$$T = C_{T1} \cdot \dot{m} \cdot \sqrt{U_d} \tag{5}$$

$$T = C_{T2} \cdot \frac{1}{L} \cdot \sqrt{U_d} \cdot hd \tag{6}$$

$$P = C_P \cdot hd \tag{7}$$

$$B = C_B \cdot \frac{1}{hd} \tag{8}$$

where $\dot{m}$ is the input mass flow rate, U_d the discharge voltage, d the channel mean diameter, h the channel width, L the channel length, and C_{T1}, C_{T2}, C_P and C_B are constants of proportionality. The trends in the data were identifieed as not perfectly linear, however mean proportionality constants have been provided[21]as C_{T1} = 1077.3, C_{T2} = 0.0924 and C_P = 1.20106. For an initial determination of thruster sizing, the assumption of linearity was deemed to be sufficient. From Equation (7), the *hd* product can be determined which can subsequently by used in Equation (6) to calculate L for a given discharge voltage U_d.

The method utilised by K. Dannenmeyer to then calculate h and d independently involves an iterative process using in-house thermal models to determine the optimum ratio between these dimensions to minimise heating and erosion. However, it has been shown that from a comparison of existing Hall Thrusters, the ratio of *h/d* remains typically constant[19], attributed to the majority of HETs having been scaled approximately linearly from the SPT-100. For the SPT-100, h/d = 0.176. By utilising this ratio, all channel dimensions can then be calculated directly for any given power and thrust input.

The proportionality constant C_B was not provided in the literature. However, as *B* and the *hd* product are known for the SPT-100 and Equation (8) shows that *B* *hd* is constant, the newly determined hd product can be used to nd the corresponding magnetic field required for the scaled thruster.

The above equations were used for the intial scaling of the thruster, with Table 4 illustrating the output parameters for a 100 W Hall thruster capable of delivering 5 mN thrust with a discharge voltage of 300 V.

Table 4. Initial thruster parameters for a 100W, 5mN thruster.

	Value
Mean Channel Diameter (mm)	21.7
Channel Width (mm)	3.8
Channel Length (mm)	26.7
Mass Flow Rate (mg/s)	0.268
Magnetic Field Strength (T)	0.306

In order to verify the validity of these scaled parameters, similarity criteria were employed. As the thruster is being designed to operate on alternative propellants, the similarity criteria for krypton, zinc and magnesium will be investigated as well as for xenon.

The mean ionisation length λ_i should be less than the channel length. The ionisation length is given by the following relation[22]:

$$\lambda_i = \frac{v_n}{n_e \langle \sigma_n v_e \rangle} \tag{9}$$

where v_n is thermal velocity of neutral atoms, n_e is the number density of electrons, σ_n is the electron impact ionisation cross section of the neutral atom and v_e is the electron thermal velocity. The product of $\sigma_n v_e$ gives the ionisation rate of neutrals. These parameters must be estimated for each propellant type in order to calculate the ionisation length.

The mean thermal velocity v of a particle in three dimensions with mass m and temperature T is given by:

$$v = \sqrt{\frac{8k_B T}{m\pi}}\ , \tag{10}$$

where k_B is the Boltzmann constant. In order to calculate the electron thermal velocity using Equation (10), the electron temperature must be determined. It has been shown that the electron temperature is a function of the discharge voltage and can be estimated by the linear relationship $T_e = 0.12U_d$ where T_e is expressed in eV [22].

An estimate of neutral temperature is required for the estimate of the neutral velocity. Multiple studies have used 800 K for the chamber temperature or neutral temperature[20,23], and will be used here to provide an estimate. The different atomic masses of the propellant will likely affect the the value of neutral temperature, but for simplicity the effect is ignored. K. Dannenmeyer states that the ionisation degree of neutral atoms is approximately 10% in a HET and therefore $n_e = 0.1n_n$ where n_n is the number density of neutral atoms.

The mass flow rate of neutrals can be expressed as:

$$\dot{m}_n = n_n \cdot m_n \cdot v_n \cdot A, \tag{11}$$

where A is the annular cross section, which can be simplifyed to $A = hd$. Rearranging Equation (11) provides a method for determining n_n once v_n has been calculated. Applying the ionisation degree then provides an estimate for the electron number density.

Separate literature sources were used to provide values of either the ionisation rate or the electron impact ionisation cross section for each propellant under study. D. Goebel provides an empirical equation of the ionisation rate of xenon as a function of T_e and v_e [22]. Approximate values from prior research for the ionisation cross section of krypton[24], zinc[25] and magnesium[26] were used within the electron temperature range 20 - 40eV.

The necessary variables can then be calculated and the ionisation length for the given thruster geometry obtained using Equation (9). Taking the ratio between the ionisation length and the channel length then provides a quantifiable measure of how well the similarity criteria is met.

A second similarity criteria is that the ion Larmor radius must remain much larger than the channel length to minimise deflection, and conversely the electron Larmor radius must be much smaller to ensure confinement. For the electron Larmor radius r_e, the thermal velocity given in Equation (10) is used as the electron's velocity. In the case of the ion radius, the ion velocity v_i is instead calculated through an energy balance:

$$v_i = \sqrt{\frac{2qU_d}{m_n}}\eta_\theta \eta_{++}\ , \tag{12}$$

where η_θ is the beam angle efficiency and η_{++} is the doubly charged ion efficiency. Using the magnetic field strength of the thruster, this similarity criteria could then be evaluated for the different propellant options.

Finally, the gyrofrequency must be much higher than the electron-atom collision frequency can be evaluated.

Table 5. Similarity criteria of the initial scaled dimensions for xenon and alternative propellants.

	Xe	**Kr**	**Zn**	**Mg**	**Criteria**
Ionisation Length Ratio	6.74×10^{-2}	8.15×10^{-2}	7.40×10^{-2}	7.03×10^{-2}	‹‹1
Electron Larmor Ratio	2.55×10^{-3}	2.55×10^{-3}	2.55×10^{-3}	2.55×10^{-3}	‹‹1
Ion Larmor Ratio	2.91	2.33	2.06	1.25	››1
Gyrofrequency Ratio	2.70×10^{4}	3.26×10^{4}	2.09×10^{4}	1.21×10^{4}	››1

Table 5 shows the results of the separate similarity criteria using the initial scaled parameters in Table 4. The results show that for each propellant the ionisation length ratio, ion Larmor ratio and gyrofrequency all demonstrate compliance with the similarity criteria for each propellant. However, the ion Larmor ratio was found to be too low. This would result in an increase in ion deflection which would potentially increase plume divergence and increase ion-channel collisions. Apart from the propellant mass, this ratio is dependent primarily on the magnetic field strength B. A decrease in B will increase this ratio whilst decreasing the electron Larmor ratio. There is sufficient margin with the electron Larmor ratios to reduce the field and still meet the similarity criteria. Consequently, it was decided to reduce the magnetic field for the final design, with a value of 0.1 T chosen and electromagnets utilised to vary the field from tis baseline number.

Xenon demonstrates best compliance with the similarity criteria, under-performing only for the gyrofrequency ratio where krypton exceeds it. This is to be expected, as all scaling methodologies and existing HETs have been designed for xenon operation. In particular, magnesium provides poor results for the similarity criteria - especially for the ion Larmor radius due to its much lighter atomic mass. Krypton appears to demonstrate the second best results followed by zinc.

Taking into consideration the initial scaling dimensions, compliance of the parameters with the similarity criteria, the manufacture of chamber parts, and the initial designs of the anode and magnetic pole, a set of final parameters for the thruster were fixed. These parameters are presented in Table 6.

Table 6. Final parameters of the HET design for 100W, 5mN operation.

	Value
Mean Channel Diameter (mm)	22.0
Channel Width (mm)	4.0
Channel Length (mm)	24.0
Mass Flow Rate (mg/s)	0.268
Magnetic Field Strength (T)	0.10

Table 7. Similarity criteria of final thruster dimensions for xenon and alternative propellants.

	Xe	**Kr**	**Zn**	**Mg**	**Criteria**
Ionisation Length Ratio	7.92×10^{-2}	9.57×10^{-2}	8.69×10^{-2}	8.25×10^{-2}	‹‹1
Electron Larmor Ratio	8.68×10^{-3}	8.68×10^{-3}	8.68×10^{-3}	8.68×10^{-3}	‹‹1
Ion Larmor Ratio	9.91	7.91	6.99	4.26	››1
Gyrofrequency Ratio	9.30×10^{4}	1.12×10^{4}	7.20×10^{3}	4.17×10^{3}	››1

The results of the similarity criteria for the final thruster design are shown in Table 7. By reducing the magnetic field, there is a marked improvement on compliance of the ion Larmor ratio without significant compromise of the other similarity criteria. Although the electron Larmor ratio increased by a factor of 3.4, the Larmor radius still remains over 100 less than the channel length and thus high electron confinement is still to be expected. The relative performance of each propellant remains unchanged, however, operation with the condensable propellants in this study now is feasible due to the increased ion Larmor radius.

A. Magnetic Circuit

For low power Hall thrusters the design of the magnetic circuit is particularly key, with overheating of the thruster, in particular the central pole a particular issue resulting from the use of some magnetic field topologies.

For low power Hall thrusters, the magnetic field is almost exclusively applied through the use of permanent magnets. These though can be difficult to ignite, and secondly the high magnetic field can have a significant effect on the low mass ions we are investigating, and consequently it was decided to go for a mix of permanent and electromagnets.

Hall thrusters typically have limited lifetime due to the erosion of the channel. For large Hall thrusters though there has been significant work to alleviate this issue through the use of magnetic shielding, involving the moving of the field line contact point to the channel to outside of the channel geometry[27]. This has dramatically increased the lifetime of large Hall thrusters. For small Hall thrusters, there has though been questions as to whether the smaller size of the channel results in a decrease in the mass utilization efficiency, with the propellant being able to escape un-ionized from around the walls of the channel. It was therefore chosen to design a non-magneticaly shielded Hall thruster.

Finite Element Method Magnetics (FEMM) 4.2 was used as the primary tool to develop the magnetic circuit. Development of the final magnetic circuit was an iterative process to generate the required field and ensure that the flux density within the soft magnetic circuit remained below its saturation. Figure 14 presents the final magnetic circuit design which was the culmination of this process.

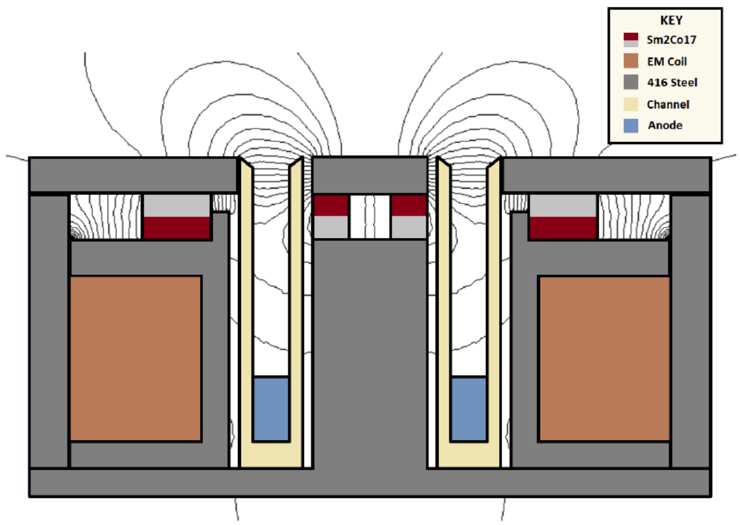

Figure 14. Cross-section of magnetic circuit design. Magnetic flux lines shown from FEMM software in the case with no current supply to the electromagnets.

B. Channel

The main parameters for design of the HET channel were the material selection and the wall thickness. The choice of material for the channel walls of the discharge chamber has been demonstrated to have a significant impact on the discharge current due to complex electron-wall interactions[28]. Alumina and boron nitride are two ceramics that have been commonly used for HET development and flight models. A comparative study of the performance of both materials on a SPT-100 displayed that both materials exhibited similar performance, except for a shift in the position of the ionisation region[29]. The physical properties of these materials are presented in Table 8.

Table 8. Comparison of physical properties of candidate wall materials.

	Density (kg/m3)	**Thermal Conductivity (W/mK)**	**Coefficient of Thermal Expansion (10^{-6}/K)**
Alumina	3550	16.9	8.2
Boron Nitride	2030	33.0	2.4

Boron nitride demonstrates superior thermal properties that are important for HET operation. A higher thermal conductivity allows the heat generated from ion bombardment to transfer away from the channel to the base plate faster, reducing the thermal stresses experienced by the channel. There will also be a high thermal loading the thruster channel, in particular when operating with condensable propellants. Boron nitride has a much lower thermal expansion, a stronger heritage of use on HETs and was cheaper to source, thus was selected as the wall material.

The life limiting factor of non-magnetically shielded thrusters is the erosion of the outer wall of the channel. As the channel width and mean diameter were fixed, the channel wall thickness was a trade-off between providing enough space for the magnetic pole and maximising wall thickness during the magnetic circuit design process. The final wall thickness was set as 1.5mm.

E. Ahedo estimates the ions sputtering rate and therefore the thruster lifetime using[30]:

$$\frac{d}{dt}(\delta h_c) = -g_r \cdot \frac{Y(\varepsilon,\theta)}{n_c}, \tag{13}$$

where $\delta h_c(t)$ is the channel wall thickness, g_r the radial ion flux to the walls, n_c the channel material density, and $Y(\varepsilon, \theta)$ the sputtering function dependent on the ion energy ε and beam divergence θ.

The equation above can be solved to calculate the approximate thruster lifetime t_{life} as:

$$t_{life} \approx \frac{h_c}{n_e T_e^{1/2}} \cdot \frac{n_c}{Y(\varepsilon,\theta)}. \tag{14}$$

Ahedo provides a typical value of $d/dt(\delta h_c)$ for a mid-power HET with boron nitride walls with U_d = 300V as 5 μm/h. Although given that this may be an underestimate for a low lower power thruster, we will use this as a starting point. The radial ion flux can be approximated by[31]:

$$g_r = 0.61 n_i v_B, \tag{15}$$

where n_i is the ion density and v_B is the Bohm velocity, the ion speed of sound, which can be calculated as;

$$v_B = \sqrt{\frac{k_B T_e}{m_n}}. \tag{16}$$

The approximation has been made that $n_i = n_e$. Using these values and the density of boron nitride, Equation (13) can be used to determine $Y(\varepsilon, \theta)$. Equation (14) can then provide and estimate of the lifetime, using the methods to determine n_e and T_e described in the discussion on sizing above. For boron nitride walls with a thickness h_c = 1.5 mm, a lifetime of 1460 hours was calculated.

C. Thermal model

Finite element models were used to estimate the temperatures of the HET components. In order to simulate the thermal conditions of the HET during operation, it was necessary to determine the magnitude of the heat loads generated by the discharge and electromagnets.

The discharge power, predominately consisting of the anode power supply, will predominately be transferred into the kinetic plume power of accelerated ions. However, there are multiple power loss mechanisms that will result in heat transfer to the thruster. The channels walls are heated by the recombination of ions and electrons at the wall surfaces. Furthermore, electrons that diffuse towards the anode will transfer thermal energy to the anode surface. Warner presents a thorough method for determining the power loss mechanisms of HET operation and consequent heat fluxes to the channel walls and anode[31]. This method was implemented for this thruster for both xenon and alternative propellants to understand how the heating behaviour might differ for propellant choice. The results of this method are shown in Table 9 and Table 10. Detailed descriptions of each power loss mechanism are described in the relevant literature.

Table 9. Power outputs as calculated from method outlined by Warner[31].

Power Outputs (W)	Xe	Kr	Zn	Mg
Ion Plume Kinetic Power	48.49	48.49	48.49	48.49
Ion Plume Thermal Power	0.58	0.58	0.58	0.58
Ion Plume Ionisation Power	2.82	3.27	2.19	1.78
Electron Plume Thermal Power	1.75	1.75	1.75	1.75
Electron Plume Kinetic Power	4.67	4.67	4.67	4.67
Ion Wall Power	15.92	15.03	14.85	13.48
Electron Wall Power	5.04	5.04	5.04	5.04
Electron Anode Thermal Power	16.67	16.67	16.67	16.67
Radiation from Excited Neutrals	8.07	8.07	8.07	8.07
Total Power	**104.02**	**103.57**	**102.32**	**100.54**

Table 10. Total power lost as heat to discharge chamber surfaces.

Heating Power (W)	Xe	Kr	Zn	Mg
Total Anode Heating	18.69	18.69	18.69	18.69
Total Wall Heating	25.00	24.11	23.93	22.56

The summation of the calculated power loss mechanisms is 100W, demonstrating that the method is a reasonable representation of the thruster behaviour. The power lost by ion combination at the walls and electron transfer of heat to the anode are the primary sources of heat generation. It is predicted that ions with lower atomic mass deliver less heat flux to the walls, which suggests the use of condensable propellants will provide better heating conditions to the chamber, however, this will be negated somewhat by the higher feed temperatures required.

It is assumed that the power lost by radiation of excited neutrals is split such that 1/2 is absorbed by the walls, 1/4 is absorbed by the anode and 1/4 emitted out the end of the chamber. The total heating power for the anode is therefore a summation of the electron anode thermal power and the share of the emitted radiation. The total wall heating power is comprised of the power lost by electrons and ions to the walls and the emitted radiation share. These values, as shown in Table 10, were then divided by the total exposed surface area of the respective component to provide a heat flux for these surfaces in W/m^2. For the channel walls, the heat flux was assumed constant throughout the whole discharge chamber. This is a simplification; in reality the heating power is likely focused on the ionisation region. The magnitude of these heat fluxes could then by used as an input for the thermal finite element model as a boundary heat flux source.

The voltage drop across the electromagnets was measured as 2.52 V for 3 A current supply, equating to a 7.56 W power dissipation across the magnets. This was also inputted into the finite element model alongside the heat fluxes. COMSOL was used to then determine the steady state solutions for HET operation.

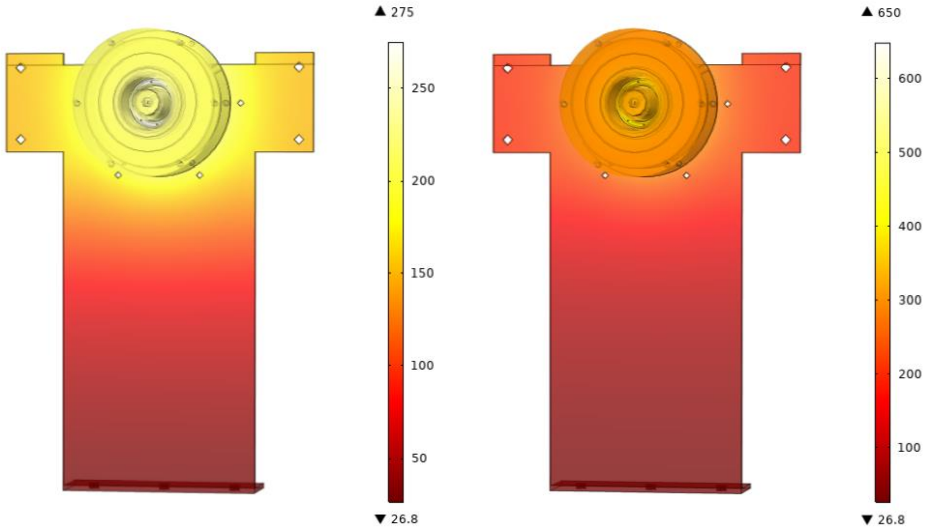

Figure 15. Temperature profile for xenon (left) and magnesium (right) operation at 100W with an electromagnet current of 3A.

Figure 15 shows the expected worst case scenarios for the HET running on xenon and magnesium respectively. In each case, the base of the HET mount has been thermally grounded at 300K. This was shown to have minimal impact to the component temperatures compared to the free floating solution. Magnesium operation represents the most extreme thermal environment due to the high temperatures required of the feed line. In these simulations, the feed line temperature was set to 650 °C, the melting point of magnesium. Likewise for zinc the feed line temperature was set at 420 °C.

The results of these simulations presented in Table 11 demonstrate that in even in the worst expected scenario, the temperature of the samarium cobalt magnets should remain within their specified operating limit of 350°C. The maximum expected magnet temperature of 327°C in all scenarios equates to a ~ 305°C change from room temperature which would result in a maximum temporary 9.15% decrease in remanence of the magnets. A less than 10% difference in the magnetic field strength should not have a significant impact on thruster operation.

Table 11. Simulated maximum steady state temperature of thruster components.

Component Temperature (°C)	**Xe**	**Kr**	**Zn**	**Mg**
Anode	275	272	346	436
Inner Channel Wall	234	231	278	333
Outer Channel Wall	231	229	274	328
Inner Magnet	230	227	273	327
Outer Magnet	218	215	256	302

D. Assembled thruster

Figure 16 illustrates the assembled thruster including channel, magnetic circuit and anode. There thruster assembled well, although it should be noted that due to a minor manufacturing error the central pole is not perfectly aligned with the centre of the channel. This will be corrected in a future iteration.

After assembly of the magnetic circuit, a transverse gaussmeter probe was used to measure the magnetic field profile of the HET. The probe was raised and lowered incrementally throughout the discharge chamber to map the change in radial magnetic flux.

Figure 16. The assembled thruster.

Figure 17 compares the results of the field measurements along the channel centreline against those predicted by the FEMM simulation. No electromagnet current was applied. The maximum field strength was measured at over 0.117 T, 1.34 times greater than the initial 0.087 T value predicted by the FEMM model. This discrepancy is due to the strength of the permanent magnets, which are producing a stronger field than that predicted. Despite this, the overall topology achieved is very similar to that predicted. The peak in flux near to the discharge chamber exit occurs in the same location to that predicted and the magnetic flux is minimal towards the anode as required for optimal performance. As expected from the FEMM simulations, a reversal in the field towards the anode was also measured.

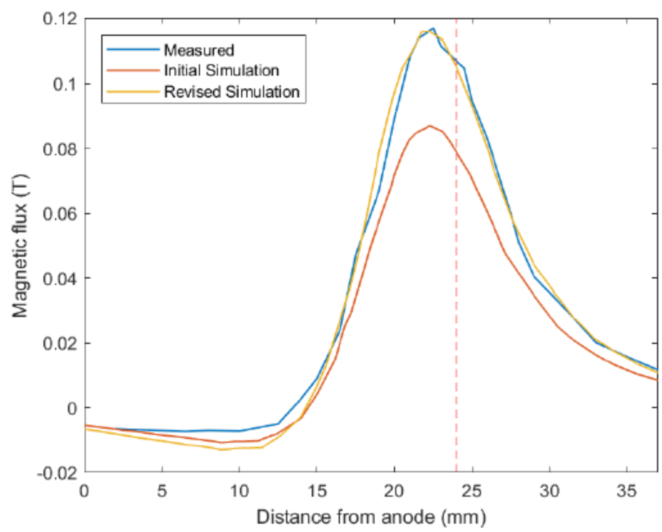

Figure 17. Comparison between measured and simulated fields along channel centreline. No electromagnet *I* applied.

Given the measured results, the properties of the Sm2Co17 magnets for the FEMM simulation were varied to better represent the system. Previously, the coercivity used for the magnets was 772 kA/m. The magnet properties provided by the manufacturer specified that the magnets hould be within 677 – 830 kA/m. Using the maximum coercivity specified and by increasing the magnetic permeability value used in the simulations from 1.103 to 1.16, a much better fit of the measured behaviour was predicted, as also illustrated in Figure 17.

E. Initial attempts at testing

The thruster was setup within the David Fearn Electric Propulsion Facility at the University of Southampton, on the same thrust stand as illustrated in ***Figure 2***. Unfortunately operation was not possible, with the hollow cathode not operating. It is hoped that this will be resolved in the next several months.

VI. Conclusion and Future Work

Significant progress has been made towards the operation of a low power Hall thruster on condensable propellants, in particular zinc and magnesium. A cylindrical Hall thruster has been developed and successfully testing on krypton, demonstrating reasonable performance. A propellant delivery system suitable for zinc has been designed, manufactured and successfully tested, demonstrating reasonable controllability at outputting suitable flow rates of zinc. A 100 W Hall Thruster, using a novel mix of permanent and electromagnets has been manufactured.

The next steps, to occur in the next few months, are to operate the cylindrical Hall thruster on zinc propellant, measuring its current voltage characteristics, and general stability. This will be followed by in depth investigation of the operation of the annular 100 W Hall thruster on krypton, and the operation of the 100 W Hall thruster on zinc. Magnesium propellant will also then be investigated, and other condensable propellants such as iodine and cadmium investigated.

The work is paving the way for a clear analysis on whether condensable propellants within low power hall thrusters are feasible, and providing much needed in depth analysis of the subject.

Acknowledgments

The authors would like to thank OHB Sweden for the continued support of this research through PhD funding.

The authors would like to thank the Engineering, Design and Manufacturing Centre at the University of Southampton for manufacturing the majority of components for the Hall thrusters used within this work.

References

1 Herman, D. A. & Unfried, K. G. Xenon Acquisition Strategies for High-Power Electric Propulsion NASA Missions, *7th JANNAF SPS Subcommittee Meeting*, Nashville, TN, GRC-E-DAA-TN23198, (2015).

2 Linnell, J. A. & Gallimore, A. D. Efficiency analysis of a hall thruster operating with krypton and xenon. *J. Propul. Power* **22**, 1402-1418 (2006).

3 Benavides, G. F., Kamhawi, H., Mackey, J., Haag, T. & Costa, G. Iodine Hall-effect electric propulsion system research, development, and system durability demonstration, *Joint Prop. Conf.*, Cincinnati, Ohio, AIAA–2018–4422, (2018).

4 Szabo, J. *et al.* Performance evaluation of an iodine-vapor Hall thruster. *J. Propul. Power* **28**, 848-857 (2012).

5 Marrese-Reading, C. *et al.* The VHITAL program to demonstrate the performance and lifetime of a bismuth-fueled very high Isp Hall thruster, *41st Joint Prop. Conf.*, Tucson, Arizona, AIAA-2005-4564, (2005).

6 Szabo, J., Robin, M. & Hruby, V. Bismuth Vapor Hall Effect Thruster Performance and Plume Experiments, *Proceedings of the the 35th International Electric Propulsion Conference*, (2017).

7 Makela, J. M., Washeleski, R. L., Massey, D. R., King, L. B. & Hopkins, M. A. Development of a magnesium and zinc Hall-Effect Thruster. *J. Propul. Power* **26**, 1029 (2010).

8 Szabo, J., Robin, M., Duggan, J. & Hofer, R. Light metal propellant Hall thrusters, *31st Int. Electric Prop. Conf.*, IEPC-2009-138, (2009).

9 Hopkins, M. A. & King, L. B. Magnesium Hall Thruster with Active Thermal Mass Flow Control. *J. Propul. Power* **30**, 637-644 (2014).

10 Tisdall, P., Dyer, E., Ryan, C., Garcia, V. & Demairé, A. Initial investigation of alternative propellants for use with a low-power cylindrical hall thruster, *Space Prop. Conf.*, Seville Spain, SP2018-333, (2018).

11 Raitses, Y., Smirnov, A. & Fisch, N. Cylindrical hall thrusters, *37th AIAA Plasmadynamics and Lasers Conference*, AIAA 2006-3245, (2006).

12 Smirnov, A., Raitses, Y. & Fisch, N. J. Experimental and theoretical studies of cylindrical Hall thrusters. *Physics of Plasmas* **14**, 057106 (2007).

13 Polzin, K., Raitses, Y., Merino, E. & Fisch, N. Preliminary results of performance measurements on a cylindrical hall-effect thruster with magnetic field generated by permanent magnets, *3rd Spacecraft Propulsion Subcommittee (SPS) meeting/JANNAF Interagency Propulsion Committee*, Orlando, Florida, M09-0186, (2008).

14 Smirnov, A., Raitses, Y. & Fisch, N. J. Plasma measurements in a 100 W cylindrical Hall thruster. *Journal of Applied Physics* **95**, 2283-2292 (2004).

15 Raitses, Y., Merino, E. & Fisch, N. J. Cylindrical Hall thrusters with permanent magnets. *Journal of Applied Physics* **108**, 093307 (2010).

16 Ryan, C., Wantock, T., Harle, T. & Knoll, A. Performance Characterization of the Low-Power Halo Electric Propulsion System. *J. Propul. Power* **32**, 1544-1549 (2016).

17 Alcock, C., Itkin, V. & Horrigan, M. Vapour pressure equations for the metallic elements: 298–2500K. *Canadian Metallurgical Quarterly* **23**, 309-313 (1984).

18 Kieckhafer, A. & King, L. B. Energetics of propellant options for high-power Hall thrusters. *J. Propul. Power* **23**, 21-26 (2007).

19 Dannenmayer, K. & Mazouffre, S. Elementary scaling relations for Hall effect thrusters. *J. Propul. Power* **27**, 236-245 (2011).

20 Dannenmayer, K. & Mazouffre, S. Elementary scaling laws for sizing up and down Hall effect thrusters: Impact of simplifying assumptions, *Proceedings of the 31st International Electric Propulsion Conference (Ann Arbor), IEPC*, (2009).

21 Dannenmayer, K. & Mazouffre, S. Sizing of Hall effect thrusters with input power and thrust level: An empirical approach. *arXiv preprint arXiv:0810.3994* (2008).

22 Goebel, D. M. & Katz, I. *Fundamentals of electric propulsion: ion and Hall thrusters*. Vol. 1 (John Wiley & Sons, 2008).

23 Barral, S., Peradzynski, Z., Makowski, K. & Dudeck, M. Model of Gas Flow Inside a Plasma Thruster, *XXI ICTAM*, Warsaw, Poland.

24 Bartlett, P. L. & Stelbovics, A. T. Calculation of electron-impact total-ionization cross sections. *Physical Review A* **66**, 012707 (2002).
25 Kaur, J., Gupta, D., Naghma, R., Ghoshal, D. & Antony, B. Electron impact ionization cross sections of atoms. *Canadian Journal of Physics* **93**, 617-625 (2014).
26 BEAMS, N. P. I. A. Absolute values of electron impact ionization cross sections for magnesium, calcium, strontium and barium. *Soviet Physics JETP* **34** (1972).
27 Hofer, R. R., Goebel, D. M., Mikellides, I. G. & Katz, I. Magnetic shielding of a laboratory Hall thruster. II. Experiments. *Journal of Applied Physics* **115**, 043304 (2014).
28 Gascon, N., Dudeck, M. & Barral, S. Wall material effects in stationary plasma thrusters. I. Parametric studies of an SPT-100. *Physics of Plasmas* **10**, 4123-4136 (2003).
29 Gascon, N., Meezan, N., Thomas, C. & Cappelli, M. Plasma Oscillations and Wall Material Effects in a Hall Thruster, *39th AIAA/ASME/SAE/ASEE Joint Propulsion Conference and Exhibit*, (2003).
30 Ahedo, E. & Gallardo, J. Scaling down Hall thrusters, *Proceedings of the 28th International Electric Propulsion Conference, Toulouse, France (paper 104)*, (2003).
31 Warner, N. Z. *Theoretical and experimental investigation of Hall thruster miniaturization*, Massachusetts Institute of Technology, (2007).